Differences in coupling between nuclear and electronic energy losses in UO2 with irradiation temperature: an in situ TEM study

A Georgesco, G Gutierrez, J.P Crocombette, C Baumier, D Drouan, C Onofri

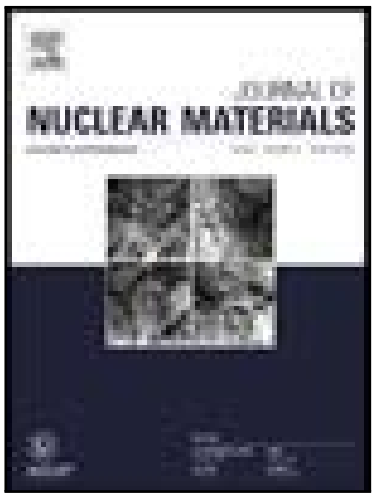

Differences in coupling between nuclear and electronic energy losses in UO_2 with irradiation temperature: an in situ TEM study

A. Georgesco , G. Gutierrez , J.-P. Crocombette , C. Baumier , D. Drouan , C. Onofri

PII: S0022-3115(24)00304-0
DOI: https://doi.org/10.1016/j.jnucmat.2024.155202
Reference: NUMA 155202

To appear in: *Journal of Nuclear Materials*

Received date: 26 January 2024
Revised date: 5 May 2024
Accepted date: 3 June 2024

Please cite this article as: A. Georgesco , G. Gutierrez , J.-P. Crocombette , C. Baumier , D. Drouan , C. Onofri , Differences in coupling between nuclear and electronic energy losses in UO_2 with irradiation temperature: an in situ TEM study, *Journal of Nuclear Materials* (2024), doi: https://doi.org/10.1016/j.jnucmat.2024.155202

Differences in coupling between nuclear and electronic energy losses in UO_2 with irradiation temperature: an *in situ* TEM study

A. Georgesco[a,*], G. Gutierrez[a], J.-P. Crocombette[a], C. Baumier[b], D. Drouan[c], C. Onofri[c]

[a]Université Paris-Saclay, CEA, Service de recherche en Corrosion et Comportement des Matériaux, SRMP, 91191Gif sur Yvette, France.

[b]Université Paris-Saclay, CNRS/IN2P3, IJCLab, Orsay, 91405, France.

[c]CEA, DES, IRESNE, DEC, Cadarache, 13108 St Paul lez Durance, France.

Abstract

To investigate the coupling between nuclear and electronic energy losses in UO_2, we irradiated thin foils with 0.39 MeV Xe and/or 6 MeV Si ions at 93 K using single or simultaneous dual beam ion irradiations. The evolution of perfect dislocation loops was characterized by *in situ* transmission electron microscopy (TEM). Additional *ex situ* TEM characterizations at room temperature revealed for the first time in UO_2 the presence of faulted Frank loops too small to be measured during *in situ* experiments and conventional bright field kinematical imaging conditions.
For the single Xe irradiation, which favor dominant ballistic energy losses, we observed a continuous nucleation of small perfect dislocation loops, which increase in size for our last fluences by growing through mainly coalescence effect. Both the single Si and dual Xe & Si irradiations showed a coupling between nuclear and electronic energy losses, resulting in a significant loop density increase and a tangled line network formation, respectively. These phenomena occur at lower dpa levels, compared to the single Xe irradiation, likely resulting from the thermal spike effect of Si ions. The present results were compared to our previous work at 293 K to investigate the role of irradiation temperature on the energy losses coupling. For the Xe irradiation, the density increases and the loops are smaller at 93 K compared to 293 K, resulting from the uranium interstitials mobility being prevented or allowed. For the Si irradiation, the dislocation evolution kinetics are similar at both temperatures. The electronic excitations effect seems greater than the irradiation temperature effect in this temperature range. For the Xe & Si irradiation, the loop kinetics change resulting in a tangled line network formation is faster and thus the loop transformation into lines occurs at lower dpa levels at 93 K compared to 293 K. It appears that the irradiation temperature affecting the mobility of some small point defects reduces the electronic excitation effect in this case.

Keywords

UO_2
In situ TEM
Ion irradiation
Dislocations
Energy losses coupling
Irradiation temperature

1. Introduction

* Corresponding author.
E-mail address: arthur.georgesco@cea.fr (A. Georgesco).

In pressurized water reactors, uranium dioxide (UO_2) is the main material used as nuclear fuel. During in-pile irradiation, it is subjected to irradiation by various particles (neutrons, fission fragments, alpha and beta particles) and radiation (gamma). Several phenomena occur simultaneously such as: radiation damage accumulation, implantation of fission products, swelling. All these phenomena, coupled with an important thermal gradient between the pellet periphery and core, lead to significant changes in the material microstructure.

The main source of irradiation damage is fission products (FPs). As they travel through matter, FPs lose energy through first mainly electronic interactions (collisions with electrons) and at the end of their path mainly by nuclear interactions (collisions with nuclei). However, in the reactor, it is difficult to know how the evolution of the microstructure is affected by the different irradiation parameters, given that they all act at the same time. It is therefore necessary to perform separate-effect studies, which is possible by using ion beam irradiations. In UO_2, according to molecular dynamics (MD) simulations, atomic displacements induced by nuclear energy losses cause cascades of collisions in the crystalline structure. These cascades generate point defects, which lead to the formation of extended defects such as interstitial dislocation loops and small vacancy objects [1–6].

In the literature, many ion irradiation studies have investigated the impact of the different irradiation parameters on the microstructure of UO_2 or surrogate materials (such as CeO_2 and ThO_2). Several TEM characterization studies have focused on the creation and evolution of dislocations through irradiation with low-energy ions [5–15] or on the formation of ion tracks through irradiation with high-energy ions [16–19]. Recently, studies on the coupling between nuclear and electronic energy losses have been carried out in UO_2 using simultaneous dual beam ion irradiations [20–22]. These studies have shown that the electronic contribution induces an acceleration of the evolution kinetics of interstitial-type loops in UO_2, and that with a sufficient level of electronic energy loss, dislocation lines can be formed at lower dpa levels. However, these studies were carried out at room temperature, where the mobility of uranium interstitial clusters [23–26] is non-negligible and can induce point defect recombination at longer range and/or loop growth through interstitial absorption. The aim of the present work is to carry out a fundamental study of the coupled effect of nuclear and electronic energy losses in UO_2, when the mobility of point defects has no or very few effect on the microstructure evolution during irradiation. It presents results obtained *in situ* by transmission electron microscopy (TEM) on thin foils irradiated with low-energy (0.39 MeV Xe) and/or "high-energy" (6 MeV Si) ions. Single and dual beam irradiations were carried out at 93 K on the JANNuS-Orsay facility. These results are also compared to the results of Bricout *et al.* [21] performed in the same conditions at 293 K in order to investigate the irradiation temperature effect.

2. Experimental procedures

Polycrystalline pellets were made by sintering depleted UO_2 powder at 1973 K for 4 h under Ar-H_2 (5 %). The pellets were cut into discs using a saw equipped with a diamond wire. After polishing of one side, they were annealed under an Ar-H_2 (5 %) atmosphere at 1973 K for 24 h. They were mirror-polished with colloidal silica suspension, and then annealed under Ar-H_2 (5 %) atmosphere at 1673 K again for 4 h in order to maintain their stoichiometry (O/U = 2.00) and remove the damage induced by polishing. The average grain size was measured at 7.6 μm and the density at 97 % of the theoretical one (i.e. 10.95 $g.cm^{-3}$). The tripod polishing technique was used to perform a mechanical thinning on the rough face, followed by a chemical etching that make use of a solution of nitric acid, glacial acetic acid and orthophosphoric acid at 393 K [27] to obtain thin UO_2 foils with electron transparent areas.

Irradiations were performed at the JANNuS-Orsay facility using the IRMA ion implantor and the ARAMIS accelerator [28] coupled with a TEM. All irradiations were conducted at 93 K to limit the defect mobility. The temperature was maintained constant at 93 K by cooling the sample holder with liquid nitrogen. The beam scanning parameters were adjusted to ensure a homogeneous fluence on the total surface of the thin foils. Irradiations were followed *in situ* using video monitoring available on-

site. Related to the previous study [21], and taking into account the available energy ranges in the JANNuS-Orsay facility, 0.39 MeV Xe and 6 MeV Si ions were selected to favor nuclear ((dE/dx_{nucl})) and electronic ((dE/dx_{elec})) energy losses in the thin foil, respectively. While 0.39 MeV Xe ions induce mainly ballistic damage, whose depth profile is well matched with the thickness of the thin foils (between 50 and 150 nm), 6 MeV Si ions are the best compromise in terms of electronic contribution. Indeed, these ions have the highest level of electronic energy losses of all the ions available in the JANNuS-Orsay facility, even if they have also a non-negligible level of nuclear energy losses in the thickness range of the thin foils. These irradiation parameters, presented on Fig. 1 and Tab. 1, were calculated using the Iradina code [29]. Atomic displacements and implanted ions profiles were determined using the full cascade mode (setting for each atom its replacement energy equal to its threshold displacement energy [30], [31]). Energy losses profiles were obtained using the ion profile only mode. The threshold displacement energies were set to 40 eV for U [32] and 20 eV for O [32,33]. All fluences were converted in dpa values, which were obtained from Iradina calculations and averaged over the measured thickness of the thin foils (around 150 nm).

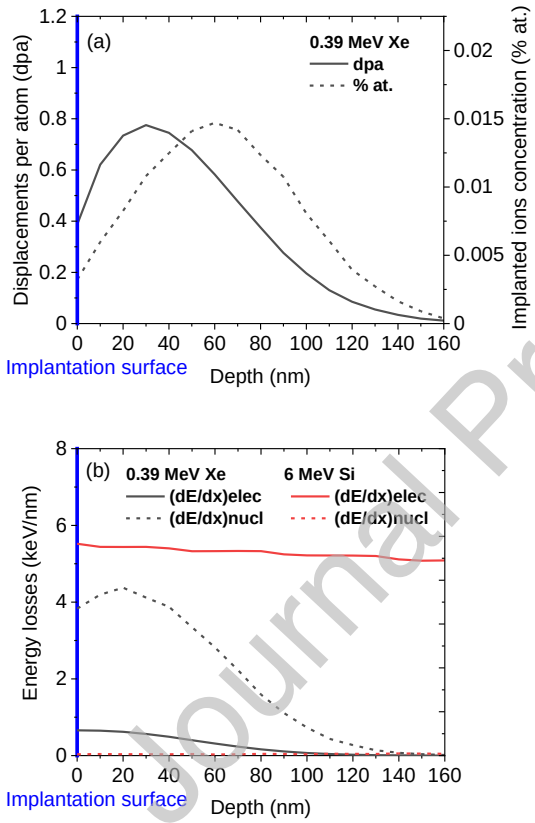

Fig. 1. Iradina calculations of (a) depth distribution of atomic displacements and implanted ions concentration calculated at the fluence of 1×10^{14} Xe/cm² and (b) depth distribution of nuclear and electronic energy losses of 0.39 MeV Xe and 6 MeV Si [29]. In this depth area, the atomic concentration of Si ions is zero and the averaged dpa value is equal to 0.01 dpa (for 1×10^{14} Si/cm²).

Tab. 1. Irradiation parameters for the Xe and Si ion beams. Energy losses and dpa values were averaged over the EELS measured thickness of the thin foils.

Ion	Xe^{3+}	Si^{3+}
Energy (MeV)	0.39	6
Ion flux ($\times 10^{11}$ ions.cm^{-2}.s^{-1})	1	2
dpa flux ($\times 10^{-4}$ dpa/s)	3.9	0.2
Elec. energy losses (keV/nm)	0.3	5.3
Nucl. energy losses (keV/nm)	2.1	0.04
Ratio of energy losses (elec/nucl)	0.1	129.5

Several fluence steps were selected for detailed observations at 93 K of the UO_2 thin foils microstructure by TEM. Various irradiations were performed:

- Single beam irradiation with 0.39 MeV Xe^{3+} ions (up to 4×10^{14} Xe/cm²), which served as the reference for nuclear damage. Due to beam time restriction, it was not possible to achieve higher fluences. However, the same irradiation was carried out in our previous work [14] in a wider fluence range and can be directly compared (dpa should be averaged over the sample thickness of 50 nm).
- Single beam irradiation with 6 MeV Si^{3+} ions (up to 7×10^{14} Si/cm²), to investigate the coupling between its predominant electronic energy losses and its own low nuclear contribution.
- Simultaneous dual-beam irradiation with both Xe and Si ions (referred to as Xe & Si) to investigate the coupling between nuclear and electronic energy losses. Fluence steps were chosen to remain in the case where the beam with the predominant electronic contribution (Si ions) does not generate its own visible defects at the TEM scale but interacts with the defects created by the high nuclear contribution of the Xe ions.

During the Xe & Si irradiation, the flux ratio between Si and Xe ion beams was maintained at a value of 2.0 ± 0.1. To prevent sample heating, the flux of 6 MeV Si ions was limited to 2.10^{11} ions.cm^{-2}.s^{-1}. During irradiation, a thermocouple, as close as possible to the thin foils, was used to monitor the temperature. Flux values in dpa, calculated with Iradina, are given in Tab. 1.

The thickness of the samples was measured by electron energy loss spectrometry (EELS) using a GIF TRIDIEM GATAN. The value of the used collection semi-angle was 5.87 mrad. Thickness was deduced from the log-ratio method using the following formula [34]:

$$t = \lambda \ln\left(\frac{I_T}{I_0}\right) \#(1)$$

Where I_T is the total intensity of the EELS spectrum, I_0 the intensity of the zero-loss peak, and λ the electron mean free path for inelastic scattering. The value of λ was set to 175 nm, according to Reyes *et al.* [35] taking into account our used collection semi-angle. Data were acquired using Gatan Digital Micrograph software. The mean thicknesses of the probed areas are about 150 nm. Uncertainties for sample thickness are set to 10 % [36].

In situ TEM characterizations were carried out during the irradiation with a 200 kV TECNAI G² 20 Twin TEM (with LaB_6 source and spatial resolution of 0.27 nm) equipped with a GATAN OneView 1095 4k x 4k camera. The loop density and average size were measured with the ImageJ software, from the characterization of between 20 and 400 loops per irradiation fluence step, with a diffraction vector $\boldsymbol{g}$ oriented along one of the cubic UO_2 ⟨220⟩ directions. According to Hirsch and Steeds [37], for fcc lattice, assuming a homogeneous loop population, the fraction of invisible dislocations with a $\frac{a}{2}\langle 110\rangle$ Burgers vectors $\boldsymbol{b}$ is about $\frac{1}{6}$ for $\boldsymbol{g}$ = 220 reflections. According to several studies performed on UO_2 irradiated with neutrons [1] or ions [5,6,11], dislocation loops (larger than about 5 nm in diameter) exhibit Burgers vectors along the ⟨110⟩ directions. According to calculations, faulted dislocation loops with Burgers vectors along the ⟨111⟩ directions exist but should be smaller than 2 nm in UO_2 [38,39]. To our knowledge, no experimental observations are available in the literature for the latter in UO_2, probably because they are too small to be observed and/or characterized by conventional bright field imaging conditions and extinction methods ($\boldsymbol{g.b}$ = 0). Indeed, very small loops (< 1 nm) often show very weak contrast or are completely invisible under bright-field kinematical imaging conditions. Rel-Rod dark field imaging technique applied in other materials, like ThO_2, allows highlighting small faulted loops [40]. This technique was applied to our samples after the ion irradiations and revealed a high density of very small faulted loops with a mean diameter of about 1 nm. During the *in situ* experiments, performed at lower magnifications, most of the characterized loops present diameter higher than 1.5 nm. Very few of these faulted loops were thus taken into account in the determination of density and average size presented in this study (less than 10 % of

them). A discussion about the magnification effect and the faulted loop characterization is available in Appendix 2. Thus, the real perfect loop density should be higher by a factor of 1.2 (for ⟨220⟩ reflections) than the one measured on the TEM images. In the paper, only real loop densities (where the factor 1.2 is applied) are presented.
As the observed dislocation loops have often an elliptical shape, their size was defined as the length of their longest axis. Uncertainty for dislocation loops densities was determined using the following formula:

$$\Delta d_{loop} \approx d_{loop}\sqrt{\left(\frac{1}{\sqrt{N}}\right)^2+\left(\frac{\Delta t}{t}\right)^2} \quad \#(2)$$

Where d_{loop} is the loop density, N the number of measured loops, t the thickness of the studied area and Δt the uncertainty for the thickness (set to 10 % of the thickness).
Uncertainty for dislocation loop average size was determined using the following formula:

$$\Delta \emptyset_{loop} \approx \emptyset_{loop}\sqrt{\left(\frac{1}{\sqrt{N}}\right)^2+\left(\frac{\Delta px}{\emptyset_{loop}}\right)^2} \quad \#(3)$$

Where $ø_{loop}$ is the loop average size and Δpx the relative pixel error on the length measurement, which was estimated to 2 pixels (about 0.9 nm for a magnification of × 50 K, and 0.6 nm for a magnification of × 80 K).

3. Results

To begin, the impact of the single beam irradiations is studied on UO_2 thin foils irradiated with either 0.39 MeV Xe (nuclear contribution) or 6 MeV Si (predominant electronic contribution) ions. Then, a second part presents the microstructure evolution with simultaneous dual Xe and Si ion beam irradiation (Xe & Si).

3.1. Single beam irradiations

3.1.1. Nuclear energy loss regime (0.39 MeV Xe ions)

The evolution of the microstructure was followed during irradiation with the video monitoring on-site. Fig. 2 displays the bright field (BF) TEM micrographs of the thin foil irradiated with 0.39 MeV Xe ions at 93 K at increasing fluences and dpa levels (up to 4×10^{14} Xe/cm² that corresponds to 1.56 dpa). The images were recorded with diffraction vectors oriented along one of the cubic UO_2 ⟨220⟩ directions. The fresh sample does not exhibit extended defects at the TEM scale (Fig. 2(a)). Starting from 4×10^{12} Xe/cm² (not shown here), dislocation loops are generated upon irradiation, appearing as small black dots with a size of a few nanometers. With the fluence increase, the loops number increases (Fig. 2(b-e)). At the final irradiation fluence (Fig. 2(e)), loops are more numerous and some of them appear to be larger in size. Nevertheless, no dislocation lines are yet observed.

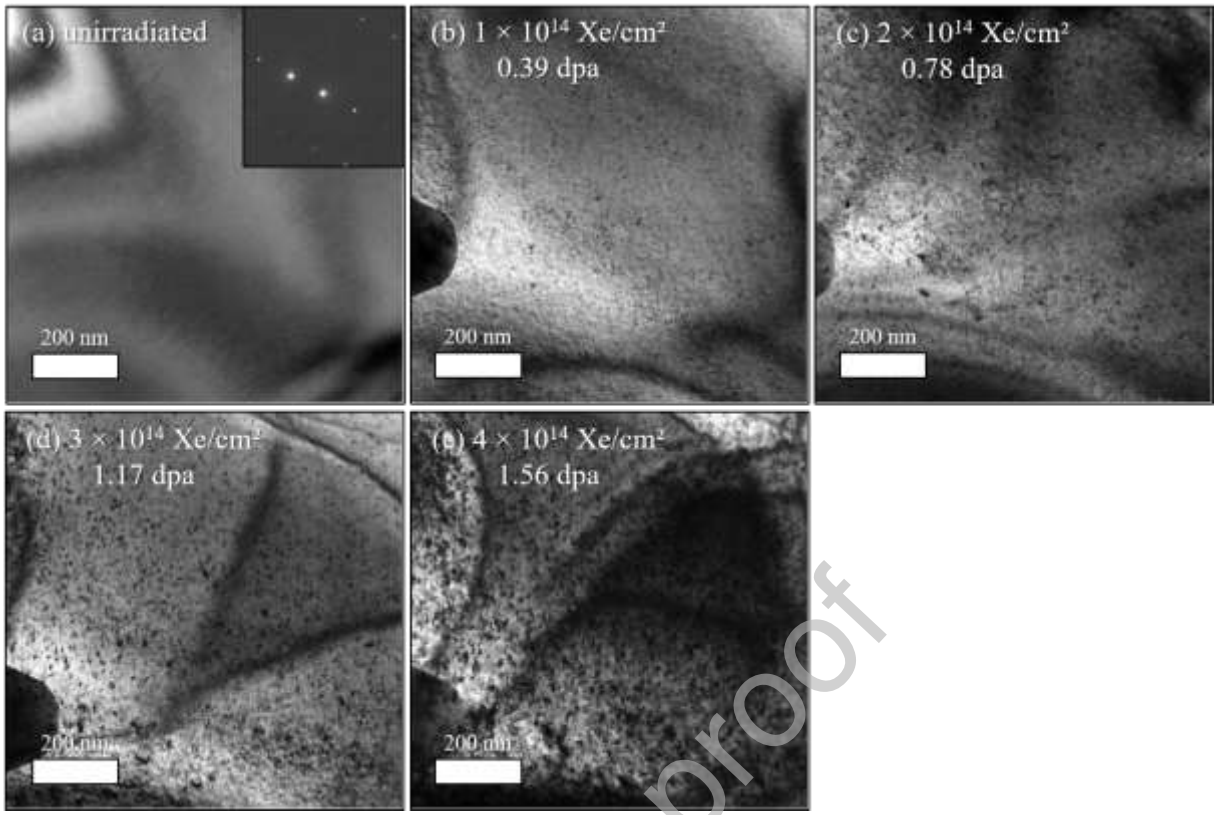

Fig. 2. BF TEM images of polycrystalline UO_2 thin foils (a) unirradiated and irradiated at 93 K with 0.39 MeV Xe ions at (b) 1×10^{14}, (c) 2×10^{14}, (d) 3×10^{14} and (e) 4×10^{14} Xe/cm². The inset shows the diffraction pattern. All dpa values were calculated with Iradina averaged on the thickness of the thin foil. The diffraction vectors are oriented along one of the cubic UO_2 ⟨220⟩ directions.

The density and sizes distribution of the dislocation loops were measured from these images and then plotted as a function of dpa (Fig. 3).

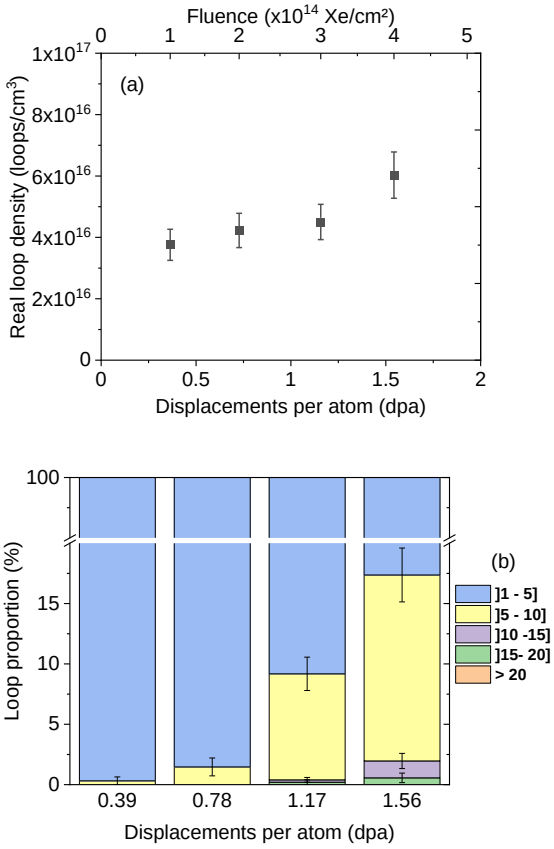

Fig. 3. (a) Evolution of the dislocation loop density and (b) distribution of loop sizes at the different dpa levels induced by irradiation with 0.39 MeV Xe ions at 93 K. Experimental values were obtained with a diffraction vector oriented along one of the cubic UO_2 ⟨220⟩ directions. The real loop density factor of 1.2 was applied to the density values.

The loop density increases with the dpa level: it rises from (3.8 ± 0.5) × 10^{16} loops/cm^3 (at 0.39 dpa) to (6.0 ± 0.7) × 10^{16} loops/cm^3 (at 1.56 dpa). Regarding the distribution of loop sizes, at 0.39 and 0.78 dpa most of the loops are smaller than 5 nm. At 1.17 dpa, larger loops with sizes ranging from 5 to 10 nm are formed, representing 8.8 ± 1.3 % of the total loops. At 1.56 dpa, this proportion has risen to 15.4 ± 2.2 %. A small proportion (< 2 %) of larger loops with sizes between 10 and 20 nm is observed at 1.17 and 1.56 dpa. Given the small proportion of larger loops at 1.17 and 1.56 dpa, the mean loop size increases slightly through the irradiation (from 2.0 ± 0.7 to 3.5 ± 0.8 nm). The results are in good agreement with our previous data [14] where the final fluence achieved was higher and the interaction of loops to form entangled dislocation lines was evidenced between 2.2 and 2.9 dpa.

3.1.2. Predominant electronic energy loss regime (6 MeV Si ions)

The microstructure evolution was also followed during the irradiation on UO_2 thin foils with 6 MeV Si ions, which have a predominant electronic contribution compared to their lower nuclear contribution. Fig. 4 shows the BF TEM micrographs of the thin foil irradiated with 6 MeV Si ions at 93 K at increasing fluences and dpa levels (up to 7 × 10^{14} Si/cm² corresponding to 0.07 dpa). The images were recorded with diffraction vectors oriented along one of the cubic UO_2 ⟨220⟩ directions. No extended defects were observed at the TEM scale before irradiation (Fig. 4(a)). At low fluences, only a few dislocations loops are visible near the edges, i.e. in the thinnest areas (less than 50 nm thick), with sizes of few nanometers (Fig. 4(b-c)). Starting from 3 × 10^{14} Si/cm², very small loops are also visible in the thicker areas (about 150 nm thick) (Fig. 4(d)). Beyond this irradiation step, the number of these small loops increases (Fig. 4(e-f)).

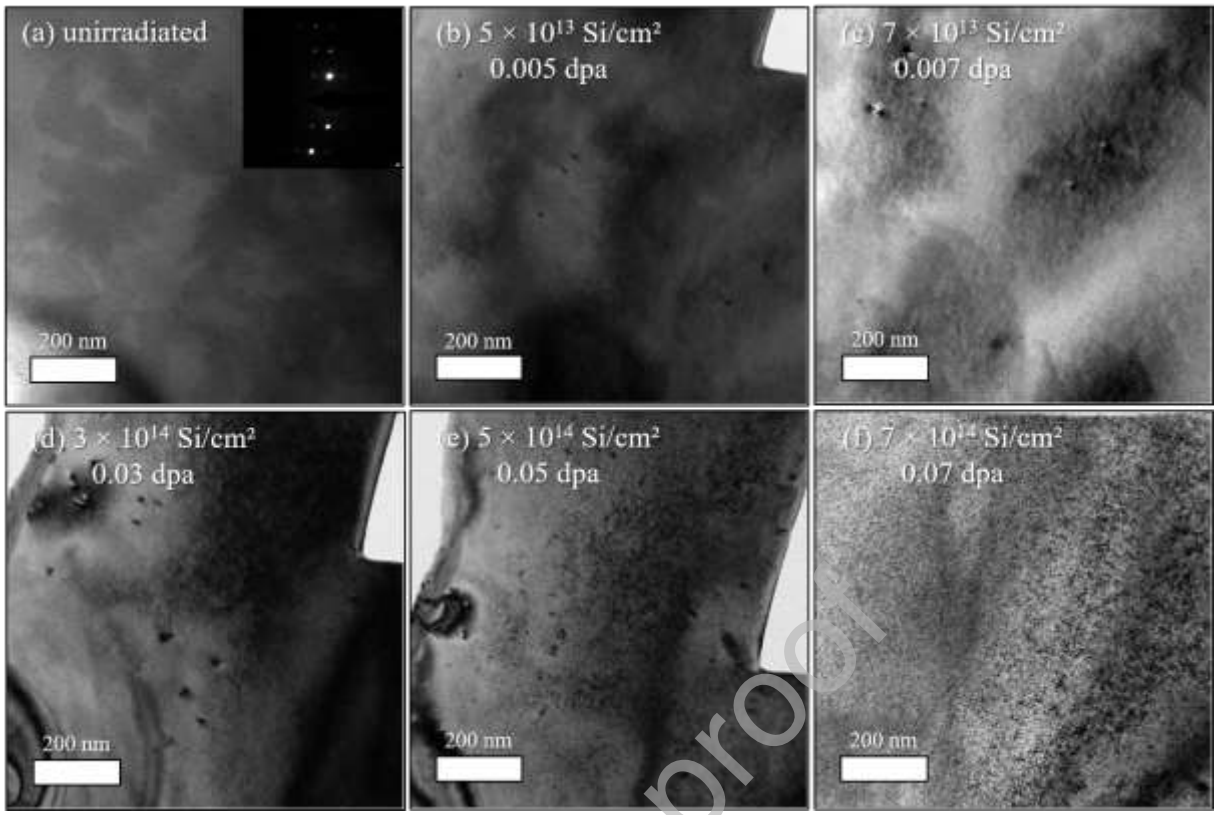

Fig. 4. BF TEM images of polycrystalline UO_2 thin foils (a) unirradiated and irradiated at 93 K with 6 MeV Si ions at (b) 7×10^{13}, (c) 3×10^{14}, (d) 5×10^{14} and (e) 7×10^{14} Si/cm². The inset shows the diffraction pattern. All dpa values were calculated with Iradina averaged on the thickness of the thin foil. The diffraction vectors are oriented along one of the cubic UO_2 ⟨220⟩ directions.

The dislocation loops were measured and their density and size distribution were determined from these images and plotted as a function of dpa (Fig. 5). The two first irradiation steps are not shown in the sizes distribution, due to the limited number of loops (less than 30 loops), which results in a non-statistical representation of their size.

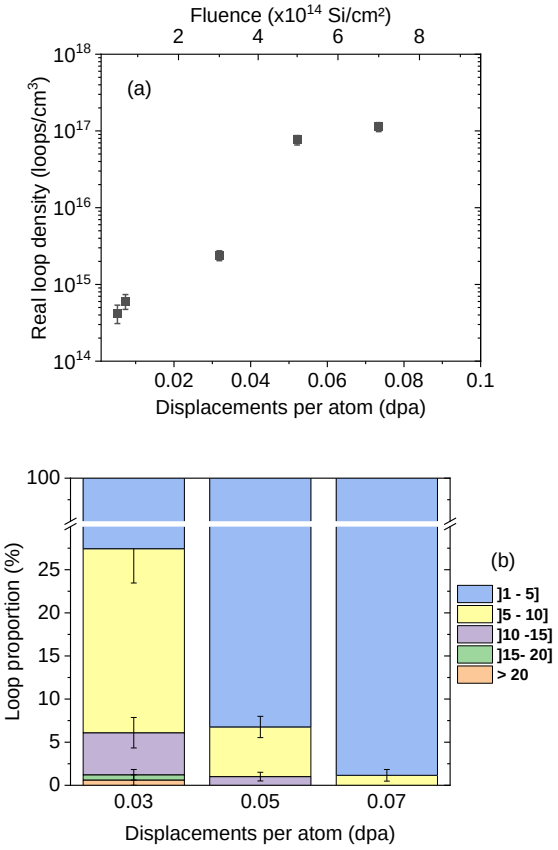

Fig. 5. (a) Evolution of the dislocation loop density on a logarithmic scale and (b) distribution of loop sizes at the different dpa levels induced by irradiation with 6 MeV Si ions at 93 K. Experimental values were obtained with a diffraction vector oriented along one of the cubic UO_2 ⟨220⟩ directions. The real loop density factor of 1.2 was applied to the density values. The sizes of the two first irradiation steps are not shown due to the limited number of loops, which results in a non-statistical representation of their size.

The loop density remains low (< 10^{15} loops/cm^3) during the first two irradiation steps. At 0.03 dpa, it rises to (2.4 ± 0.4) × 10^{15} loops/cm^3 as the small loops have started to nucleate/be visible at the TEM scale in the thicker areas. Between 0.03 and 0.05 dpa, the loop density increases, reaching a value of (7.6 ± 1.0) × 10^{16} loops/cm^3, and it continues to rise until the end of the irradiation ((1.1 ± 0.2) × 10^{17} loops/cm^3). Regarding the distribution of the loop sizes, at 0.03 dpa, the distribution shows the presence of larger loops with sizes between 5 and 20 nm, which are formed since the beginning of the irradiation in the thinnest areas. Starting from 0.05 dpa, the proportion of these loops decreases due to the high number of smaller loops being formed in thicker areas. At 0.07 dpa, the proportion of these small loops now represents almost all of the observed loops (98.8 ± 8.7) %. Note that, the contrast as well as the apparent size of the small loops (< 10 nm) can change according to the foil thickness and the depth of the loop in the foil [41]. For example, dislocation loops lying close to the foil surface often show black–white contrast and are often sized from dynamic two-beam micrographs, whereas loops lying towards the center of thicker foils do not show well-developed black–white contrast and appear as black dots (e.g. under kinematical bright-field conditions, or when they lie between or outside the black–white layers). These different contrasts can lead to more or less variations in the measured loop diameter. However, some studies in other materials [42] have also shown that the nature and size of the loops induced during ion irradiations in temperature can vary according to the thickness of the zone studied. To limit free surface effects on loop characteristics, it seems important to study thick samples, especially in temperature.

It is important to take into account the Si dpa value from which the density of loops created by Si increases significantly. Indeed, in the case of the Xe & Si dual beam irradiation, the proportion of loops created by Si above this limit becomes non-negligible. It can lead to a misrepresentation of the

effect of Si electronic contribution on Xe ballistic damage. In the present case, the limit has been determined at 0.03 dpa (3×10^{14} Si/cm²) for the Si beam.

3.2. Dual beam irradiation

After studying the independent single beam effect for each contribution, the dual beam Xe & Si irradiation was performed. Fig. 6 presents the BF TEM micrographs of the thin foil irradiated simultaneously with both 0.39 MeV Xe and 6 MeV Si ions at 93 K at increasing fluences and dpa levels (up to 2×10^{14} Xe/cm² or 0.80 dpa). The flux ratio between Si and Xe ion beams was maintained at a value of 2.0 ± 0.1. The images were recorded with diffraction vectors oriented along one of the cubic UO_2 ⟨220⟩ directions. At low fluences, few dislocations loops appear, with sizes of a few nanometers (Fig. 6(b)). Starting from 5×10^{13} Xe/cm², numerous dislocation loops are formed (Fig. 6(c)). As the irradiation progresses, the loops number increases (Fig. 6(d-e)). At the final irradiation fluence of 2×10^{14} Xe/cm², the dislocation loops transform into a network of tangled lines, with the remaining presence of large dislocation loops, which have not yet be transformed into lines (Fig. 6(f)). The appearance of the first lines was observed experimentally using video monitoring on-site at 1.6×10^{14} Xe/cm² (or 0.65 dpa), indicating that the transformation of loops into lines occurred rapidly between 1.6×10^{14} and 2×10^{14} Xe/cm².

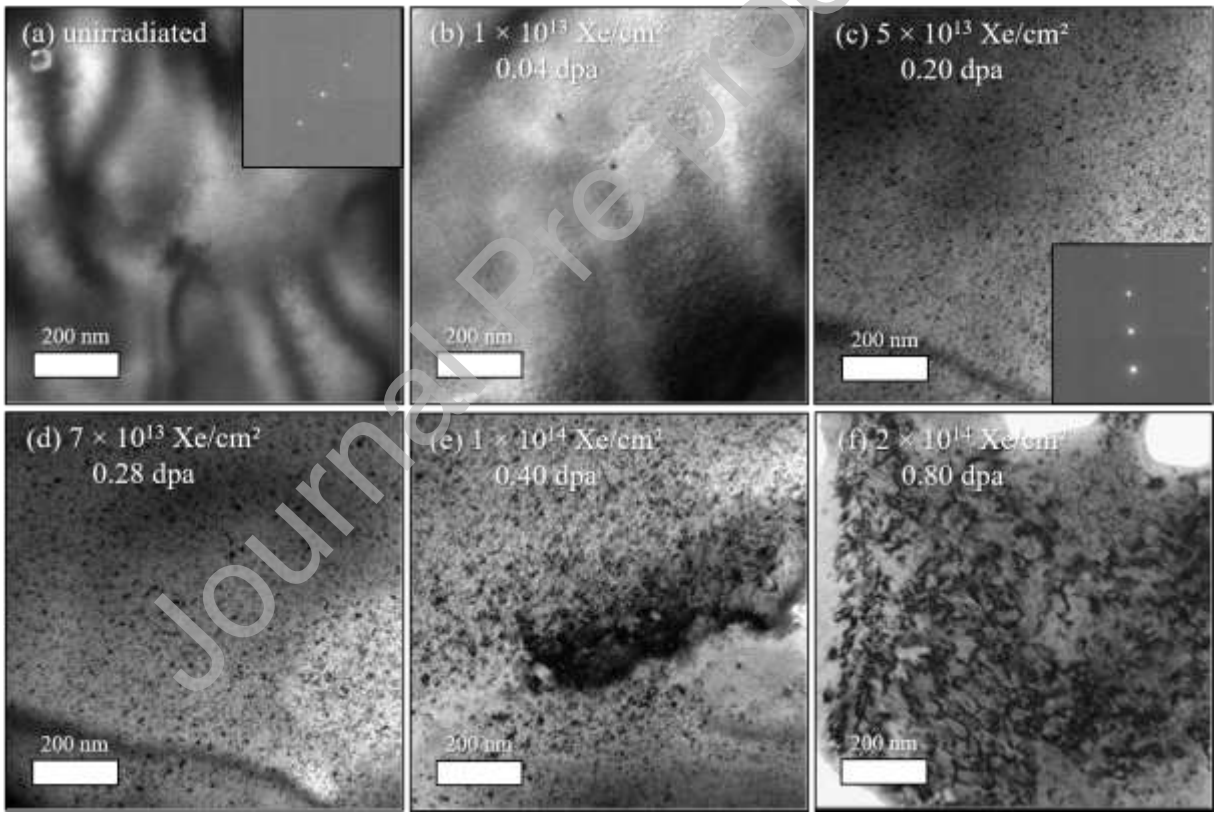

Fig. 6. BF TEM images of polycrystalline UO_2 thin foils (a) unirradiated and irradiated at 93 K with simultaneous dual 0.39 MeV Xe and 6 MeV Si ion beam at (b) 1×10^{13}, (c) 5×10^{13}, (d) 7×10^{13}, (e) 1×10^{14} and (f) 2×10^{14} Xe/cm². The insets show the diffraction patterns. All dpa values were calculated with Iradina averaged on the thickness of the thin foil, Xe and Si dpa values being added up. The diffraction vectors are oriented along one of the cubic UO_2 ⟨220⟩ directions. Due to the breaking of the first studied area during irradiation, images (a) – (b) and (c) – (f) were taken at different areas of the thin foil.

The dislocation loops were measured and their density and sizes distribution were extracted from these images and plotted as a function of dpa (Fig. 7). For each fluence step, Xe and Si dpa values were added up.

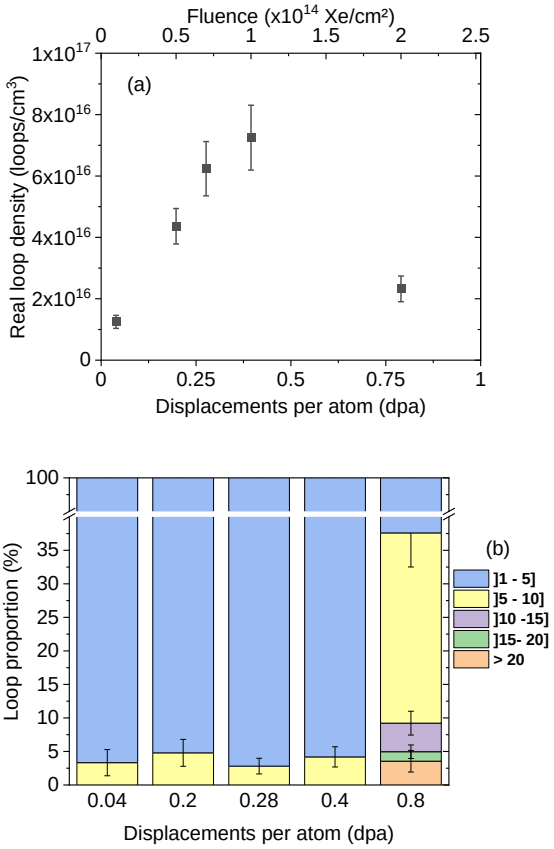

Fig. 7. (a) Evolution of the dislocation loop density and (b) distribution of loop sizes at the different dpa levels induced by irradiation with simultaneous dual 0.39 MeV Xe and 6 MeV Si ion beam at 93 K. Experimental values were obtained with a diffraction vector oriented along one of the cubic UO_2 ⟨220⟩ directions. The real loop density factor of 1.2 was applied to the density values. In Equation (2), as the first term governs the other two terms, the density uncertainties for the first and last points are lower.

As observed on the micrographs, the loop density increases rapidly between 0.04 and 0.40 dpa. At 0.40 dpa, the density reaches its maximum value of $(7.2 \pm 1.0) \times 10^{16}$ loops/cm^3. Between 0.40 and 0.80 dpa, a significant decrease in density is observed, corresponding to the transformation of loops into lines, decreasing their density to $(2.3 \pm 0.4) \times 10^{16}$ loops/cm^3. Regarding the distribution of loop sizes, between 0.04 and 0.40 dpa, most of the loops observed have sizes smaller than 5 nm. A small proportion of larger loops with sizes between 5 and 10 nm are highlighted. At 0.80 dpa, the proportion of small loops (< 5 nm) is significantly reduced (62.4 ± 8.4 %) and much larger loops, up to > 20 nm, are now observed. This increase corresponds to the presence of the large dislocation loops that have interact and thus grown but not yet transformed into lines.

4. Discussion

4.1. Coupling between nuclear and electronic energy losses at 93 K

To investigate the coupling between nuclear and electronic energy losses, single and dual ion beam irradiations were performed using 0.39 MeV Xe and/or 6 MeV Si ions at 93 K. Fig. 8 gathers the loop/line density evolutions of the single Xe, Si and dual Xe & Si ion beam irradiations, plotted as a function of fluence and dpa.

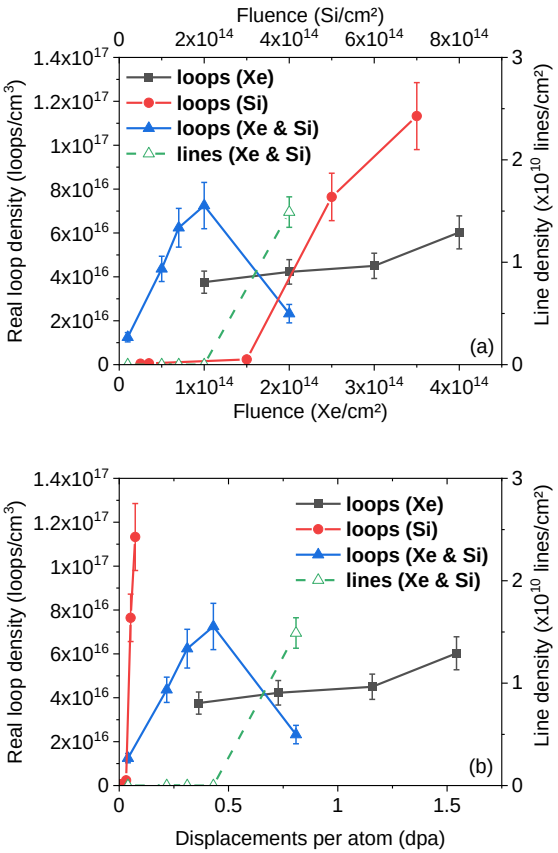

Fig. 8. Evolution of the dislocation loop/line density during irradiation with 0.39 MeV Xe and/or 6 MeV Si ion beam at 93 K as a function of (a) dpa (b) fluence. All dpa values were calculated with Iradina averaged on the thickness of the thin foil, Xe and Si dpa values being added up in the case of Xe & Si. Experimental values were obtained with a diffraction vector oriented along one of the cubic UO_2 ⟨220⟩ directions. The real loop density factor of 1.2 was applied to the density values.

During the sole Xe irradiation (Fig. 8(a), black curve), small dislocation loops with sizes between 1.5 and 5 nm are mostly formed. Given the peaked nature of the Xe damage profile (Fig. 1), it is likely that the distribution of loops as a function of depth is not uniform and that most of the loops form in the first 100 nm of the thin foil with a maximum at about 30 nm, which matches the thickness of the thin foils. In our previous work [11], we showed that there is no loop denuded zone near edges of the sample irradiated at 93 K, indicating that the free surfaces have a limited effect on the loop density at this temperature. Their average size remains globally stable (2 – 3 nm) between 0.39 and 1.56 dpa, while the loop density increases. These results are in good agreement with the previous *in situ* observations performed on UO_2 lamella also irradiated with 0.39 MeV Xe under the same low temperature conditions [14]: a continuous nucleation of small loops (< 5 nm), up to a high density value at around 2.2 dpa, before the loop interaction and formation of a tangled line network. In our work, a slight growth of the loop size is observed at 1.56 dpa whereas the loop density achieves a high value, so it is reasonable to believe that the loop interaction is close to occur as observed in our previous experiment [14]. As our final irradiation step is at 1.56 dpa, we should expect a transformation of loops into lines starting after our last fluence, although we would have needed to increase the damage level to witness the transformation. At 93 K, all point defects in UO_2 have no or very low mobility [23–25]. Thus, the loop formation/growth by interstitial absorption should be limited. Therefore, it is likely that the loops are formed mostly into the collision cascade at 93 K. Given the small sizes of the loops and their limited growth, the material should be able to contain many loops before they interact for geometric reason. When the loops encounter each other, it is likely they grow by coalescence effect. The evolution of the dislocation loop density for the Xe & Si irradiation (Fig. 8(a), blue curve) occurs faster in fluence than the one of the sole Xe irradiation (Fig. 8(a), black curve). Indeed, between 0 and 0.80 dpa, the Xe & Si irradiation induces the creation and

the growth of dislocation loops until the loops transform into lines (Fig. 8(a), green curve). The significant decrease of the blue curve matches the increase of the green curve, highlighting the loops transformation into lines. On the contrary, in the case of the Xe irradiation, between 0 and 1.56 dpa the loop density evolution is still in the phase of loop nucleation and beginning of their growth. Moreover, at a close level of damage around 0.8 dpa (Fig. 2(c) for Xe and Fig. 6(f) for Xe & Si), the dislocation populations of both microstructures are very different for equivalent thicknesses. Indeed, the microstructure after Xe irradiation contains numerous dislocation loops with no presence of any lines, whereas the microstructure after Xe & Si irradiation is already a tangled lines network. One effect of the coupling between nuclear and electronic energy losses highlighted here is an acceleration of the dislocation evolution kinetics. This result is consistent with the results of previous works on the coupling between nuclear and electronic energy losses in UO_2 [20–22].

The increase of the dislocation loop density for the sole Si irradiation (Fig. 8(a), red curve) reaches higher loop density values but occurs later in fluence than for the dual Xe & Si irradiation. However, the levels of dpa induced by Si ions are much lower (Fig. 8(b), red curve) compared to Xe & Si, and even to Xe. Indeed, the microstructure exhibits numerous dislocations loops starting from 0.03 to 0.07 dpa (Fig. 4(d-f)).The differences observed can be explained by different phenomena induced by the Si ions. It induces electronic excitations and ionizations, enhancing a thermal spike along the ion path, in a uniform manner over the entire thickness of the thin foil (Fig. 1). In the hot zone, the point defects diffusion is enhanced. In the case of the single Si irradiation, the significant effect of electronic energy losses from Si ions induces recombination and clustering directly inside the collision cascade. This effect is sufficient to ensure that the Si ions induce greater loop nucleation. However, as the Si ions generate very low dpa compared to the Xe ions, the effect occurs later in fluence (at least 3×10^{14} Si/cm²). For a proper comparison between 6 MeV Si and 0.39 MeV Xe irradiations it is necessary to take into account the effect of the exogenous Xe atoms, which stop into the UO_2 matrix in the latter case. Based on our previous study [14], by comparing the dislocation evolution kinetics induced by 4 MeV Au and 0.39 MeV Xe ions at 93 K, it is assumed that the effect of exogenous Xe atoms on the loop evolution kinetics is negligible at 93 K. Indeed, 4 MeV Au have been selected to create the same amount of ballistic damage as Xe into the thin foil, but the large majority of Au atoms go through the thin samples without stopping into the UO_2 matrix. Thus, the difference is likely due to the electronic effect and not to the effect of exogenous Xe atoms at this temperature.

In the case of the dual Xe & Si irradiation, the effect of the electronic energy losses from Si ions occurs both inside and outside the Si collision cascade. Indeed, the Si ions interact also with small defects already created by the Xe ions. The defects may recombine or cluster to generate new extended defects visible at the TEM scale. Therefore, the coupling between nuclear and electronic energy losses occurs mostly outside the Si collision cascade and promotes the loop density increase, resulting in an acceleration of the transformation of dislocation loops into lines.

In summary, it is worth stressing that an irradiation using the Si ions alone or simultaneously with low energy ions induces a different coupling between nuclear and electronic energy losses. The first case results in a coupling effect occurring mostly inside the collision cascade. The second case results in a coupling effect occurring both inside and outside the collision cascade, where the Si ions interact mostly with the defects generated by the Xe ions.

4.2. Irradiation temperature effect

To investigate the irradiation temperature effect, the results from the present work were compared to the results of the previous work of Bricout *et al.* [21]. They studied the coupling between nuclear and electronic energy losses in UO_2, through single and dual beam irradiations at 293 K, using the same ions as the present study. Their density and dpa values were recalculated (see Appendix 1).

Fig. 9 compares the loop evolution of the density and average size between 93 and 293 K for the sole Xe irradiation. Concerning the global evolutions of the loop density and average size, it appears that the density is higher and the average size is slightly smaller (taking into account the uncertainties) at

93 K compared to 293 K. In contrast to 93 K, where the uranium interstitials mobility is very low, at 293 K, they have an enhanced mobility [23–26]. It could justify different mechanisms of interstitial-type loop nucleation and growth depending on the temperature.

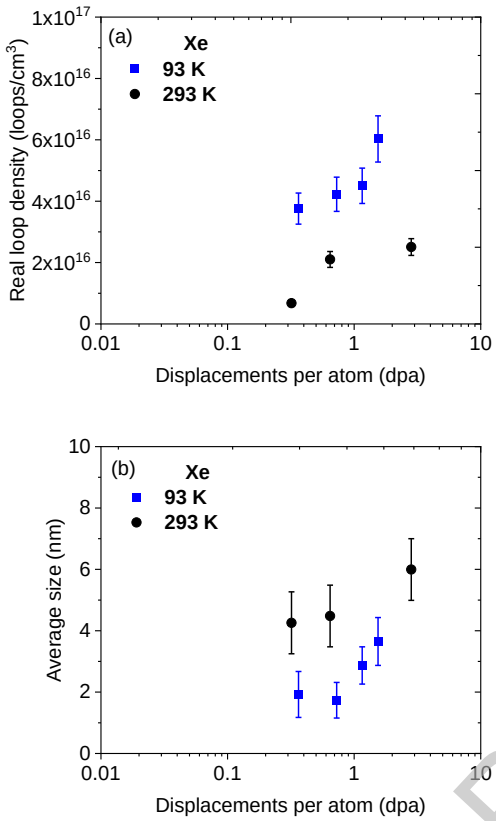

Fig. 9. Evolution of the dislocation loop (a) density and (b) average size as a function of dpa during irradiation with 0.39 MeV Xe ion beam at 93 K (present study) and 293 K (Bricout *et al.* [21]). Experimental values were obtained with a diffraction vector oriented along one of the cubic UO_2 ⟨220⟩ directions. The real loop density factor of 1.2 was applied to the density values. The thickness of the UO_2 thin foils were about 150 nm at 93 K and 50 nm at 293 K.

At 93 K, it is likely that the loop nucleation occurs mostly inside the collision cascade. Given the low mobility of the uranium interstitials, they may only recombine with uranium vacancies or cluster with their closest neighbor defects. It could explain why the loops are more numerous and have smaller sizes: a continuous nucleation occurs inside the collision cascade during the irradiation, but the generated loops have a limited growth. It is likely that the loops grow mostly by coalescence effect, when the density reaches high values, as a dislocation geometric covering occurs. On the contrary, at 293 K, the nucleation may occur both inside and outside the collision cascade, as the enhanced mobility of uranium interstitial may allow them to cluster more easily. However, they may also recombine or be absorbed by loops more easily. It may explain why the loops are less numerous and have larger sizes: the loop growth may be enhanced by interstitial absorption, and so less interstitials may be available to cluster and form new loops. It is likely that the loops grow mostly by interstitial absorption at the beginning of the irradiation. In summary, for the nuclear contribution alone, at 93 K the smaller size of the loops may allow the material to contain more of them. After reaching a high saturation density value, the loops may grow rapidly through coalescence effects. In contrast, at 293 K the enhanced mobility of uranium interstitials may induce the formation of larger loops, but given their size the material can contain less loops before they interact or annihilate. These results are in good agreement with the literature results on the temperature effect at low dpa [5,7,11]. Note that free surface effects may be more significant at 293 K compared to 93 K. In our previous work [11], a loop depleted area about tens nanometers thick was highlighted in the edge areas for irradiations performed at 293 K, whereas at 93 K loops were observed in these thin edge zones. As point defects are more

mobile, the closest to surfaces may disappear more easily with free surfaces. Furthermore, if the elastic interaction energy of the loops with the surface is sufficiently high, surface image forces cause the prismatic loop to glide to the surface and disappear. Therefore, free surfaces may affect the final loop size and density values at 293 K.

Fig. 10 presents the comparison of loop density evolution between 93 and 293 K for the dual Xe & Si and single Si irradiations.

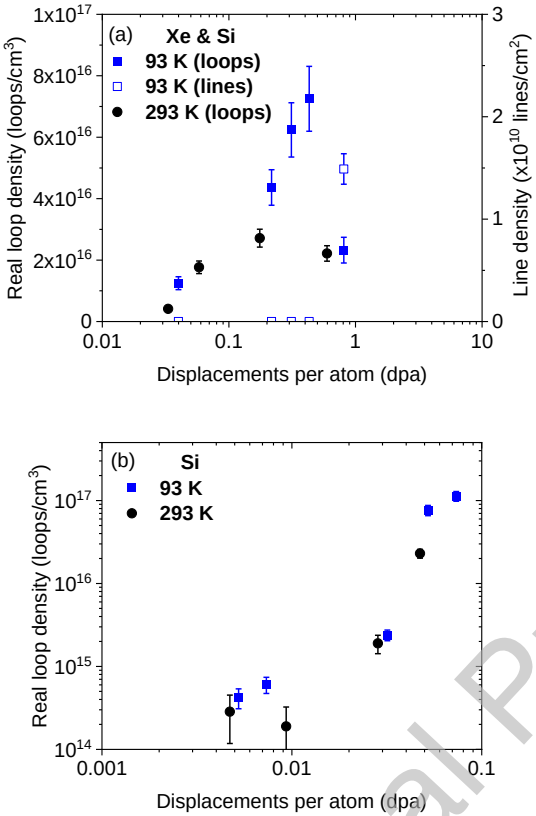

Fig. 10. Evolutions of the dislocation loop density as a function of dpa during irradiation with (a) simultaneous dual 0.39 MeV Xe and 6 MeV Si ion beams and (b) single 6 MeV Si ion beam at 93 K (present study) and 293 K (Bricout *et al.* [21]) on a logarithmic scale. Experimental values were obtained with a diffraction vector oriented along one of the cubic UO_2 ⟨220⟩ or ⟨111⟩ directions. For the Xe & Si irradiations, the real loop density factor of 1.2 was applied to the density values. For the Si irradiations, factors of 1.2 and 2 were applied respectively to the 93 K (g = 220) and 293 K (g = 111) density values, as the fraction of invisible dislocations is ½ for g = 111 reflections [37]. The thickness of the UO_2 thin foils were about 170 nm at 93 K and 70 nm at 293 K.

On the one hand, for the dual Xe & Si irradiation, at both 93 and 293 K it appears that the dislocation evolution kinetics is accelerated compared to the single Xe irradiation. However, for a similar level of damage (around 0.7 – 0.8 dpa, which corresponds to the final irradiation step of the present work), the dislocation populations differ. Indeed, at 93 K a tangled line network is already observed (Fig. 6(f)), while in the case of 293 K the loops have not yet transformed into lines [21]. Thus, it seems that the irradiation temperature influences the coupling between nuclear and electronic energy losses, as the lines transformation appeared to occur later at 293 K than at 93 K. As mentioned before, the irradiation temperature induces different dislocation populations for the sole Xe irradiation at 93 and 293 K. Therefore, when the Si ions interact with the defects generated by the Xe ions, it is possible that the mobility of uranium interstitial point defects (prevented or allowed depending on the irradiation temperature) induces different nucleation and growth evolutions in both cases (93 and 293 K, respectively). At 93 K, it is likely that most of uranium interstitials do not recombine before their interaction with Si ions. Conversely, at 293 K, it is likely that a part of uranium interstitials have already been absorbed by sinks, recombined with uranium vacancies or disappeared with free surfaces, leaving less interstitials available for the microstructure evolution. It may explain why the final

microstructures are different for a same level of Xe damage. Thus, it is consistent with the larger loop sizes observed at 293 K by Bricout *et al.* [21], compared to the present work at 93 K.
On the other hand, for the single Si irradiation, at both 93 and 293 K it appears that the loop nucleation is very important and reaches higher density values than in the case of the single Xe irradiation. However, the density and size evolutions are quite similar for the two temperatures. Thus, in this case, the effect of irradiation temperature may be negligible compared to the effect of electronic energy losses, which is occurring directly inside the collision cascade.
Finally, it is worth stressing that the effect of irradiation temperature on the coupling between nuclear and electronic energy losses appears to differ in both cases. In the case of Xe & Si, it is possible that irradiation temperature has an effect on the amount of available uranium interstitials (generated in the Xe cascade), resulting in different microstructures before and after their interaction with Si ions. Conversely, in the case of Si alone, it seems that the effect of irradiation temperature becomes negligible compared to the effect of electronic energy losses in this temperature range.

5. Conclusion

Ion beam irradiations were performed at the JANNuS-Orsay facility to study the coupling between nuclear and electronic energy losses in UO_2 at 93 K in order to have a low mobility of point defects (oxygen/uranium interstitials and vacancies). *In situ* TEM characterizations were carried out to follow the dislocation evolution under three different irradiation conditions. The effect of the irradiation temperature was also investigated through comparison of the present results with the results obtained at 293 K by Bricout *et al.* [21]. Single beam irradiations were performed to investigate the effect of either the nuclear (0.39 MeV Xe) or the predominant electronic (6 MeV Si) contribution. A simultaneous dual beam irradiation was carried out to study the coupling between both contributions.
The nuclear contribution at 93 K shows a continuous nucleation of small perfect loops (with sizes mainly between 1.5 and 5 nm), which may grow through coalescence effect when the loop number reaches a high density limit. Additional *ex situ* TEM characterizations at room temperature revealed for the first time in UO_2 the presence of faulted Frank loops too small to be evidenced during *in situ* experiments and conventional bright field kinematical imaging conditions. A coupling between nuclear and electronic energy losses was observed for both the single Si and dual Xe & Si irradiations: higher values of loop density and the formation of tangled dislocation lines at lower damage levels compared to the sole Xe irradiation, respectively. It is likely that the electronic energy losses of Si ions induce a thermal spike effect. In the case of the sole Si irradiation, it results in recombination and clustering inside the Si collision cascade. In the case of the Xe & Si irradiation, it interacts mostly with the defects generated by the Xe ions, outside the Si collision cascade.
Then, the irradiation temperature effect on the nuclear contribution appears to increase the loop density and decrease the loop average size at 93 K compared to 293 K. It seems that the limited mobility of uranium interstitials results in a prevented loop growth in the first case, while in the second case the loop growth is enhanced but the loop nucleation is more limited. It also appears that loop nucleation occurs mostly inside the cascade at 93 K, while it may occur both inside and outside at 293 K due to the enhanced mobility of uranium interstitials.
Finally, it appears that the irradiation temperature has an effect on the coupling between nuclear and electronic energy losses. The Xe & Si irradiations show the transformation of dislocation loops into lines occurring at lower dpa levels at 93 K compared to 293 K. It seems that the irradiation temperature affects the recombination and clustering of small point defects before the Si ions interact with them. Conversely, the Si irradiations show a similar dislocation evolution kinetics between 93 and 293 K. It appears that the effect of electronic excitations is greater than irradiation temperature effect in this range.

Appendix 1

The thickness of the thin foils, affecting the dislocation loop densities and averaged dpa values, used from the previous study of Bricout *et al.* [21] have been recalculated according to the recent study of Reyes *et al.* [35]. The authors compared experimental data obtained in UO_2 to different models to calculate the electron mean free path for inelastic scattering according to the collection semi-angle used, for the sample thickness measurements by EELS. They recommended to use the Jin model using the mean atomic number instead of the effective atomic number. Therefore, for a value of the collection semi-angle equal to 11.81 mrad, the modified Jin model gives the value of λ equal to 145 nm for the data of Bricout *et al.* [21].

Appendix 2

Additional *ex situ* TEM measurements were performed in order to investigate the presence of faulted loops, with Burgers vectors along the ⟨111⟩ directions. To identify these faulted loops, the Rel-Rod dark field imaging technique, as described in [40], was used at a high-magnification in order to better resolve small objects. This technique allows imaging the loops using fine-structure diffraction effects associated with the stacking faults. The magnification effect on the loop characteristics was also studied on this occasion. The UO_2 thin foils were characterized at room temperature, after irradiation, with a FEI TALOS TEM operating at 200 kV at the LECA-STAR facility in CEA Cadarache, France (spatial resolution in TEM mode of 0.19 nm). The results of these additional characterizations are presented in Fig. A1:

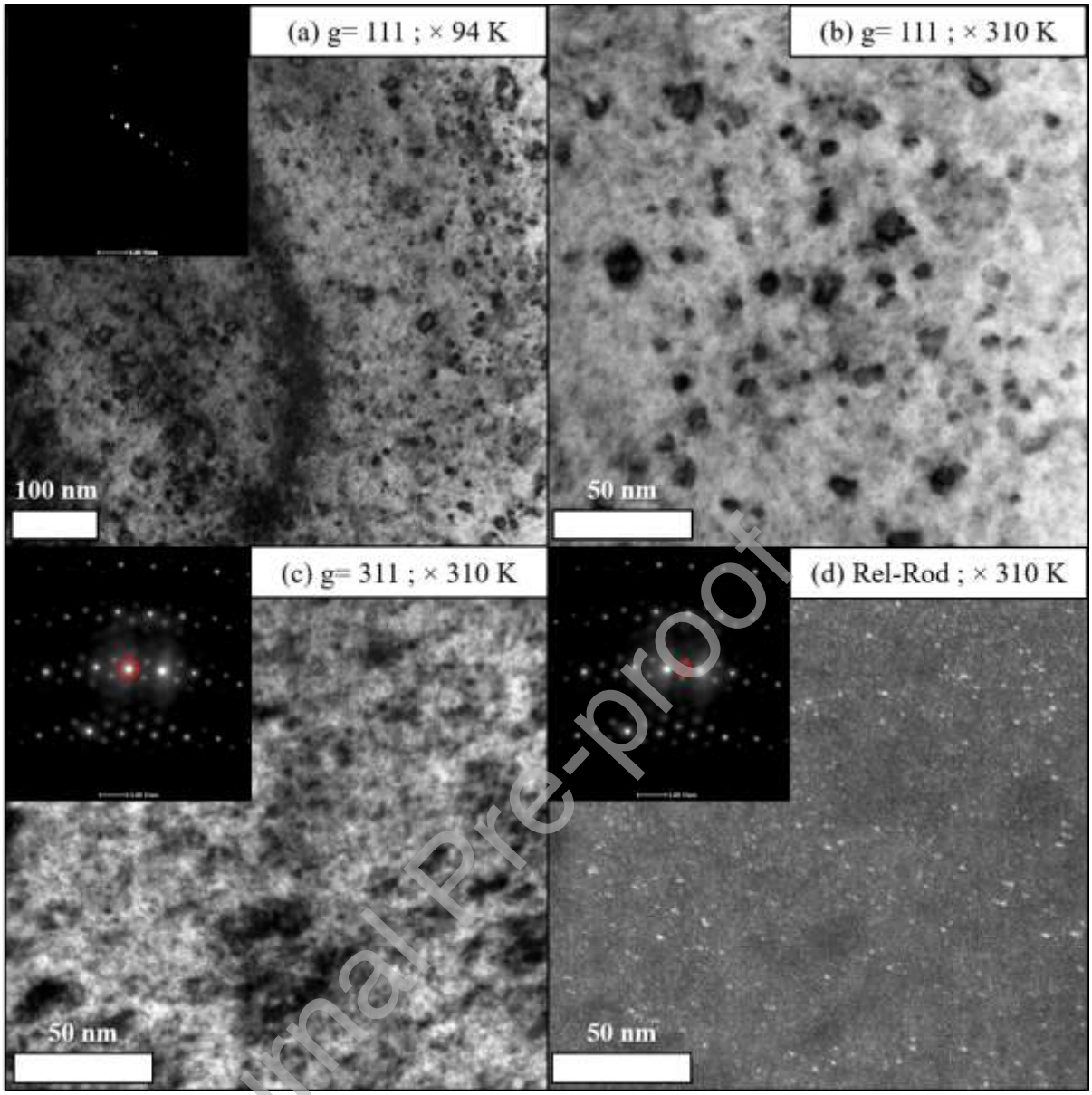

Fig. 11. TEM images of polycrystalline UO_2 thin foils at 293 K after irradiation at 93 K with simultaneous dual 0.39 MeV Xe and 6 MeV Si ion beams at 2×10^{14} Xe/cm². Images were recorded in BF mode with diffraction vectors oriented along one of the cubic UO_2 ⟨111⟩ directions (a–b), and ⟨311⟩ directions (c). (d) Image was recorded in DF mode with Rel-Rod condition. The insets show the diffraction patterns.

The Rel-Rod DF technique clearly reveals the presence of small faulted loops with Burgers vectors along the ⟨111⟩ directions (Fig. A1(d)) which present very weak contrast or are completely invisible under BF imaging conditions (Fig. A1(b, c)). The measured density is found at $(1.4 \pm 0.1) \times 10^{17}$ loops/cm^3. Regarding their size, although difficult to measure, the average size is about 1.0 nm, and all faulted loops have a diameter of less than 2 nm, in good agreement with calculations [38,39]. Size distribution of these faulted loops obtained in Rel-Rod DF mode (Fig. A1(d)) was compared to the one obtained in BF mode (Fig. A1(b)) with a diffraction vector along the ⟨111⟩ direction at the same magnification. Then, to study the effect of magnification on the loop size distribution, measurements were also conducted at a lower magnification (Fig. A1(a)). Finally, all these values were compared to the ones obtained *in situ* at low-magnification in order to state if faulted loops have been mistaken with perfect loops. The different loop size distributions are represented on Fig. A2:

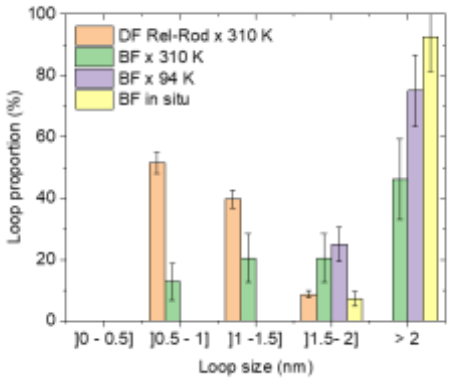

Fig. 12. Distribution of loop sizes for different imaging conditions and magnifications: BF mode with a diffraction vector oriented along one of the cubic UO_2 ⟨111⟩ directions at × 94 K (Fig. A1(a)) or × 310 K (Fig. A1(b)), BF mode in *in situ* low-magnification condition, and Rel-Rod DF condition at × 310 K (Fig. A1(d)).

To begin, the Rel-Rod DF distribution (where only faulted loops are measured) shows that, although a small proportion of loops (about 10 %) have a size larger than 1.5 nm, most of the loops (about 90 %) have a size between 0.5 and 1.5 nm. The BF high-magnification (× 310 K) distribution shows that about 50 % of the counted loops have a size larger than 2 nm, and therefore are expected to be perfect loops with Burgers vectors along the ⟨110⟩ directions. The BF low-magnification (× 94 K) distribution shows that all the measured loops have a size larger than 1.5 nm, with most of the loops (> 75 %) being larger than 2 nm. This result is not surprising since magnification has an impact both on the resolution limit and on counting statistics. Finally, the BF *in situ* distribution also obtained at a low-magnification shows that only about 10 % of the counted loops have a diameter between 1.5 and 2 nm, corresponding to possible faulted loops. Therefore, the decrease of magnification reduces the number of faulted loops mistaken with perfect loops, since the latter are mainly smaller than 1.5 nm and it is difficult to resolve such small objects at low-magnification. It appears that only a small proportion of faulted loops may have been counted as perfect loops. This proportion is estimated to be less than 10 % of the total of counted loops in this work.

Acknowledgments

Experiments performed at the IJCLab facility: JANNuS-Orsay (IJCLab, CNRS/IN2P3, Université Paris-Saclay, Orsay, France). This experiment was supported by the EMIR&A French accelerator network. This research did not receive any specific grant from funding agencies in the public, commercial, or not-for-profit sectors.

References

[1] A.D. Whapham, B.E. Sheldon, Radiation damage in uranium dioxide, The Philosophical Magazine: A Journal of Theoretical Experimental and Applied Physics 12 (1965) 1179–1192. https://doi.org/10.1080/14786436508228669.

[2] J. Soullard, Mise en évidence de boucles de dislocation imparfaites dans des échantillons de bioxyde d'uranium irradiés, Journal of Nuclear Materials 78 (1978) 125–130. https://doi.org/10.1016/0022-3115(78)90511-1.

[3] K. Nogita, K. Une, Thermal Recovery of Radiation Defects and Microstructural Change in Irradiated UO2 Fuels, Journal of Nuclear Science and Technology 30 (1993) 900–910. https://doi.org/10.1080/18811248.1993.9734564.

[4] T. Sonoda, M. Kinoshita, I.L.F. Ray, T. Wiss, H. Thiele, D. Pellottiero, V.V. Rondinella, Hj. Matzke, Transmission electron microscopy observation on irradiation-induced microstructural evolution in high burn-up UO2 disk fuel, Nuclear Instruments and Methods in Physics Research

Section B: Beam Interactions with Materials and Atoms 191 (2002) 622–628. https://doi.org/10.1016/S0168-583X(02)00622-5.
[5] L.-F. He, M. Gupta, C.A. Yablinsky, J. Gan, M.A. Kirk, X.-M. Bai, J. Pakarinen, T.R. Allen, In situ TEM observation of dislocation evolution in Kr-irradiated UO2 single crystal, Journal of Nuclear Materials 443 (2013) 71–77. https://doi.org/10.1016/j.jnucmat.2013.06.050.
[6] C. Onofri, M. Legros, J. Léchelle, H. Palancher, C. Baumier, C. Bachelet, C. Sabathier, Full characterization of dislocations in ion-irradiated polycrystalline UO2, Journal of Nuclear Materials 494 (2017). https://doi.org/10.1016/j.jnucmat.2017.07.043.
[7] B. Ye, M.A. Kirk, W. Chen, A. Oaks, J. Rest, A. Yacout, J.F. Stubbins, TEM investigation of irradiation damage in single crystal CeO2, Journal of Nuclear Materials 414 (2011) 251–256. https://doi.org/10.1016/j.jnucmat.2011.03.052.
[8] B. Ye, A. Oaks, M. Kirk, D. Yun, W.-Y. Chen, B. Holtzman, J.F. Stubbins, Irradiation effects in UO2 and CeO2, Journal of Nuclear Materials 441 (2013) 525–529. https://doi.org/10.1016/j.jnucmat.2012.09.035.
[9] W.-Y. Chen, J. Wen, M. Kirk, Y. Miao, B. Ye, B. Kleinfeldt, A. Oaks, J. Stubbins, Characterization of dislocation loops in CeO2 irradiated with high energy Krypton and Xenon, Philosophical Magazine 93 (2013). https://doi.org/10.1080/14786435.2013.838007.
[10] L.F. He, J. Pakarinen, M.A. Kirk, J. Gan, A.T. Nelson, X.-M. Bai, A. El-Azab, T.R. Allen, Microstructure evolution in Xe-irradiated UO2 at room temperature, Nuclear Instruments and Methods in Physics Research Section B: Beam Interactions with Materials and Atoms 330 (2014) 55–60. https://doi.org/10.1016/j.nimb.2014.03.018.
[11] C. Onofri, C. Sabathier, C. Baumier, C. Bachelet, H. Palancher, M. Legros, Evolution of extended defects in polycrystalline Au-irradiated UO2 using in situ TEM: Temperature and fluence effects, Journal of Nuclear Materials 482 (2016). https://doi.org/10.1016/j.jnucmat.2016.10.011.
[12] C. Onofri, C. Sabathier, H. Palancher, G. Carlot, S. Miro, Y. Serruys, L. Desgranges, M. Legros, Evolution of extended defects in polycrystalline UO2 under heavy ion irradiation: combined TEM, XRD and Raman study, Nuclear Instruments and Methods in Physics Research Section B: Beam Interactions with Materials and Atoms 374 (2016) 51–57. https://doi.org/10.1016/j.nimb.2015.08.091.
[13] Y. Haddad, L. Delauche, A. Gentils, F. Garrido, In situ characterization of irradiation-induced microstructural evolution in urania single crystals at 773 K, Nuclear Instruments and Methods in Physics Research Section B: Beam Interactions with Materials and Atoms 435 (2018) 25–30. https://doi.org/10.1016/j.nimb.2017.12.019.
[14] C. Onofri, C. Sabathier, C. Baumier, C. Bachelet, H. Palancher, B. Warot-Fonrose, M. Legros, Influence of exogenous xenon atoms on the evolution kinetics of extended defects in polycrystalline UO2 using in situ TEM, Journal of Nuclear Materials 512 (2018) 297–306. https://doi.org/10.1016/j.jnucmat.2018.10.025.
[15] L. He, T. Yao, K. Bawane, M. Jin, C. Jiang, X. Liu, W.-Y. Chen, J.M. Mann, D.H. Hurley, J. Gan, M. Khafizov, Dislocation loop evolution in Kr-irradiated ThO2, Journal of the American Ceramic Society 105 (2022) 5419–5435. https://doi.org/10.1111/jace.18478.
[16] T. Wiss, Hj. Matzke, C. Trautmann, M. Toulemonde, S. Klaumünzer, Radiation damage in UO2 by swift heavy ions, Nuclear Instruments and Methods in Physics Research Section B: Beam Interactions with Materials and Atoms 122 (1997) 583–588. https://doi.org/10.1016/S0168-583X(96)00754-9.
[17] Hj. Matzke, P.G. Lucuta, T. Wiss, Swift heavy ion and fission damage effects in UO2, Nuclear Instruments and Methods in Physics Research Section B: Beam Interactions with Materials and Atoms 166–167 (2000) 920–926. https://doi.org/10.1016/S0168-583X(99)00801-0.
[18] T. Sonoda, M. Kinoshita, N. Ishikawa, M. Sataka, A. Iwase, K. Yasunaga, Clarification of high density electronic excitation effects on the microstructural evolution in UO2, Nuclear Instruments and Methods in Physics Research Section B: Beam Interactions with Materials and Atoms 268 (2010) 3277–3281. https://doi.org/10.1016/j.nimb.2010.06.015.
[19] N. Ishikawa, T. Sonoda, T. Sawabe, H. Sugai, M. Sataka, Electronic stopping power dependence of ion-track size in UO2 irradiated with heavy ions in the energy range of ∼1MeV/u, Nuclear

Instruments and Methods in Physics Research Section B: Beam Interactions with Materials and Atoms 314 (2013) 180–184. https://doi.org/10.1016/j.nimb.2013.05.038.
[20] M. Bricout, C. Onofri, A. Debelle, Y. Pipon, R. Belin, F. Garrido, F. Lepretre, G. Gutierrez, Radiation damage in uranium dioxide: Coupled effect between electronic and nuclear energy losses, Journal of Nuclear Materials 531 (2020). https://doi.org/10.1016/j.jnucmat.2019.151967.
[21] M. Bricout, G. Gutierrez, C. Baumier, C. Bachelet, D. Drouan, F. Garrido, C. Onofri, Synergy of electronic and nuclear energy depositions on the kinetics of extended defects formation in UO2, based on in situ TEM observations of ion-irradiation-induced microstructure evolution, Journal of Nuclear Materials 554 (2021). https://doi.org/10.1016/j.jnucmat.2021.153088.
[22] G. Gutierrez, M. Bricout, F. Garrido, A. Debelle, L. Roux, C. Onofri, Irradiation-induced microstructural transformations in UO2 accelerated upon electronic energy deposition, Journal of the European Ceramic Society (2022). https://doi.org/10.1016/j.jeurceramsoc.2022.05.039.
[23] W.J. Weber, Thermal recovery of lattice defects in alpha-irradiated UO2 crystals, Journal of Nuclear Materials 114 (1983) 213–221. https://doi.org/10.1016/0022-3115(83)90259-3.
[24] A. Turos, Hj. Matzke, S. Kwiatkowski, Recovery stages in UO2 at low-temperatures, Physical Review Letters 65 (1990) 1215–1218. https://doi.org/10.1103/PhysRevLett.65.1215.
[25] Hj. Matzke, A. Turos, Ion implantation studies of UO2 and UN, Journal of Nuclear Materials 188 (1992) 285–292. https://doi.org/10.1016/0022-3115(92)90486-5.
[26] X.-Y. Liu, D.A. Andersson, Small uranium and oxygen interstitial clusters in UO2: An empirical potential study, Journal of Nuclear Materials 547 (2021) 152783. https://doi.org/10.1016/j.jnucmat.2021.152783.
[27] A.J. Manley, Transmission electron microscopy of irradiated U02 fuel pellets, Journal of Nuclear Materials 27 (1968) 216–224. https://doi.org/10.1016/0022-3115(68)90125-6.
[28] A. Gentils, C. Cabet, Investigating radiation damage in nuclear energy materials using JANNuS multiple ion beams, Nuclear Instruments and Methods in Physics Research Section B: Beam Interactions with Materials and Atoms 447 (2019) 107–112. https://doi.org/10.1016/j.nimb.2019.03.039.
[29] J.-P. Crocombette, C. Van Wambeke, Quick calculation of damage for ion irradiation: implementation in Iradina and comparisons to SRIM, EPJ Nuclear Sci. Technol. 5 (2019) 7. https://doi.org/10.1051/epjn/2019003.
[30] Y.-R. Lin, S.J. Zinkle, C.J. Ortiz, J.-P. Crocombette, R. Webb, R.E. Stoller, Predicting displacement damage for ion irradiation: Origin of the overestimation of vacancy production in SRIM full-cascade calculations, Current Opinion in Solid State and Materials Science 27 (2023) 101120. https://doi.org/10.1016/j.cossms.2023.101120.
[31] G. Gutierrez, H. Guessous, D. Gosset, M. Bricout, I. Monnet, F. Garrido, C. Onofri, G. Adroit, A. Debelle, Defect evolution under intense electronic energy deposition in uranium dioxide, Journal of Nuclear Materials 578 (2023) 154375. https://doi.org/10.1016/j.jnucmat.2023.154375.
[32] J. Soullard, High voltage electron microscope observations of UO2, Journal of Nuclear Materials 135 (1985) 190–196. https://doi.org/10.1016/0022-3115(85)90077-7.
[33] C. Meis, A. Chartier, Calculation of the threshold displacement energies in UO2 using ionic potentials, Journal of Nuclear Materials 341 (2005) 25–30. https://doi.org/10.1016/j.jnucmat.2005.01.001.
[34] R.F. Egerton, Electron Energy-Loss Spectroscopy in the Electron Microscope, Springer US, Boston, MA, 2011.
[35] D. Reyes, M. Angleraud, C. Onofri, D. Drouan, C. Sabathier, Electron inelastic mean free path in UO2 and (U, Pu)O2 fuels, Acta Materialia 248 (2023) 118779. https://doi.org/10.1016/j.actamat.2023.118779.
[36] H.-R. Zhang, R.F. Egerton, M. Malac, Local thickness measurement through scattering contrast and electron energy-loss spectroscopy, Micron 43 (2012) 8–15. https://doi.org/10.1016/j.micron.2011.07.003.
[37] P.B. Hirsch, J.W. Steeds, in: NPL Symposium No. 15, HMSO, London, 1964: p. 39. https://doi.org/10.1515/9783110842807-003.
[38] A. Chartier, C. Onofri, L. Van Brutzel, C. Sabathier, O. Dorosh, J. Jagielski, Early stages of irradiation induced dislocations in urania, Applied Physics Letters 109 (2016). https://doi.org/10.1063/1.4967191.

[39] A. Le Prioux, P. Fossati, S. Maillard, T. Jourdan, P. Maugis, Empirical potential simulations of interstitial dislocation loops in uranium dioxide, Journal of Nuclear Materials 479 (2016) 576–584. https://doi.org/10.1016/j.jnucmat.2016.07.046.
[40] K. Bawane, X. Liu, T. Yao, M. Khafizov, A. French, J.M. Mann, L. Shao, J. Gan, D.H. Hurley, L. He, TEM characterization of dislocation loops in proton irradiated single crystal ThO2, Journal of Nuclear Materials 552 (2021) 152998. https://doi.org/10.1016/j.jnucmat.2021.152998.
[41] D. Williams, C. Carter, Transmission Electron Microscopy: A Textbook for Materials Science, 2009. https://doi.org/10.1007/978-1-4757-2519-3.
[42] K. Ma, B. Décamps, L. Huang, R.E. Schäublin, J.F. Löffler, A. Fraczkiewicz, M. Nastar, F. Prima, M. Loyer-Prost, Impact of micro-alloying in ion-irradiated nickel: From the inhibition of point-defect cluster diffusion by thermal segregation to the change of dislocation loop nature, Acta Materialia 246 (2023) 118656. https://doi.org/10.1016/j.actamat.2022.118656.

Declaration of interests

☒The authors declare that they have no known competing financial interests or personal relationships that could have appeared to influence the work reported in this paper.

☐The authors declare the following financial interests/personal relationships which may be considered as potential competing interests: